Am J Physiol Endocrinol Metab 306: E469–E482, 2014.
First published December 17, 2013; doi:10.1152/ajpendo.00330.2013.

Skeletal muscle mitochondrial uncoupling drives endocrine cross-talk through the induction of FGF21 as a myokine

Susanne Keipert,[1,3]* Mario Ost,[1]* Kornelia Johann,[1] Francine Imber,[1] Martin Jastroch,[3] Evert M. van Schothorst,[2] Jaap Keijer,[2] and Susanne Klaus[1]

[1]*German Institute of Human Nutrition, Potsdam-Rehbruecke, Germany;* [2]*Department of Human and Animal Physiology, Wageningen University, Wageningen, The Netherlands; and Institute for Diabetes and Obesity, Helmholtz Zentrum München, Munich, Germany*[3]

Submitted 13 June 2013; accepted in final form 11 December 2013

Keipert S, Ost M, Johann K, Imber F, Jastroch M, van Schothorst EM, Keijer J, Klaus S. Skeletal muscle mitochondrial uncoupling drives endocrine cross-talk through the induction of FGF21 as a myokine. *Am J Physiol Endocrinol Metab* 306: E469–E482, 2014. First published December 17, 2013; doi:10.1152/ajpendo.00330.2013.—UCP1-Tg mice with ectopic expression of uncoupling protein 1 (UCP1) in skeletal muscle (SM) are a model of improved substrate metabolism and increased longevity. Analysis of myokine expression showed an induction of fibroblast growth factor 21 (FGF21) in SM, resulting in approximately fivefold elevated circulating FGF21 in UCP1-Tg mice. Despite a reduced muscle mass, UCP1-Tg mice showed no evidence for a myopathy or muscle autophagy deficiency but an activation of integrated stress response (ISR; eIF2α/ATF4) in SM. Targeting mitochondrial function in vitro by treating C_2C_{12} myoblasts with the uncoupler FCCP resulted in a dose-dependent activation of ISR, which was associated with increased expression of FGF21, which was also observed by treatment with respiratory chain inhibitors antimycin A and myxothiazol. The cofactor required for FGF21 action, β-klotho, was expressed in white adipose tissue (WAT) of UCP1-Tg mice, which showed an increased browning of WAT similar to what occurred in altered adipocyte morphology, increased brown adipocyte markers (UCP1, CIDEA), lipolysis (HSL phosphorylation), and respiratory capacity. Importantly, treatment of primary white adipocytes with serum of transgenic mice resulted in increased UCP1 expression. Additionally, UCP1-Tg mice showed reduced body length through the suppressed IGF-I-GH axis and decreased bone mass. We conclude that the induction of FGF21 as a myokine is coupled to disturbance of mitochondrial function and ISR activation in SM. FGF21 released from SM has endocrine effects leading to increased browning of WAT and can explain the healthy metabolic phenotype of UCP1-Tg mice. These results confirm muscle as an important endocrine regulator of whole body metabolism.

fibroblast growth factor 21; browning; energy metabolism; uncoupling protein 1; myokine

ECTOPIC EXPRESSION IN SKELETAL MUSCLE (SM) of uncoupling protein 1 (UCP1), the mitochondrial uncoupling protein of brown adipose tissue (BAT), leads to increased energy expenditure, delayed diet-induced obesity development, reduced hepatic steatosis, improved glucose homeostasis, and increased longevity in these muscle-specific UCP1-transgenic (Tg) mice (22, 34, 38, 50). The exact physiological mechanisms underlying this metabolic improvement have not yet been resolved. Respiratory uncoupling affected the function of not only muscle itself but also white adipose tissue (WAT), which showed an increased metabolic activity and increased insulin-stimulated glucose uptake (32, 50). This suggests cross-talk between muscle and WAT that is possibly mediated by myokines. Muscle is considered a secretory organ, secreting several hundred products. It is suggested that the beneficial health effects of exercise training could be mediated in part by secretion of such myokines that could counteract harmful effects of proinflammatory cytokines released, e.g., by WAT (52). This is supported by the recent identification of the novel myokine irisin, which is released during exercise and leads to the induction of UCP1 expression and a BAT-like development in WAT linked to improvements in obesity and glucose homeostasis in mice (6). As in exercise, UCP1 induced SM respiratory uncoupling leads to an activation of AMP-activated protein kinase (AMPK) (50) mediating increased fatty acid oxidation in muscle (33).

Fibroblast growth factor 21 (FGF21) is a unique member of the FGF superfamily subgroup that also includes FGF19/15 and FGF23. Rather than being a growth factor, it is a pleotropic hormone-like circulating protein that functions as a major metabolic regulator of glucose and lipid metabolism (7, 27, 35, 49). Circulating FGF21 is thought to be secreted primarily by the liver (3, 51). Hepatic FGF21 expression and secretion are induced largely by fasting and ketogenic diets through activation of PPARα and play an important role in the adaptation to starvation (15, 28, 41). The biological activity of FGFs is dependent on their binding to FGF receptors (FGFR) and the coreceptor β-Klotho (KLB). KLB is crucial for FGF21 specificity (27) and its metabolic action (2, 14). FGF21 expression in muscle is induced by hyperinsulinemia in humans (26), and it has been suggested to be a novel insulin-stimulated myokine (52). Interestingly, FGF21 overexpression in mice leads to a phenotype that very much resembles that of UCP1-Tg mice with ectopic UCP1 in SM, i.e., a reduced body weight and size despite normal or even increased food intake, improved glucose homeostasis (29, 36), and increased energy expenditure and longevity (63). Systemic administration of FGF21 was further shown to reduce diet-induced as well as genetic obesity (8) and is being considered as a potential therapeutic in obesity, diabetes, and related disorders.

Here, we aimed to explore whether the healthy metabolic phenotype of Tg mice expressing UCP1 in SM is linked to an induction and release of myokines, focusing on FGF21. We show that expression and secretion of FGF21 are highly induced in the SM of UCP1-Tg mice, leading to more than fivefold increased circulating levels of FGF21. This is accom-

* These authors contributed equally to this work.

Address for reprint requests and other correspondence: S. Keipert, Institute for Diabetes and Obesity, Helmholtz Zentrum München, Parkring 13, 85748 Garching, Munich, Germany (e-mail: susanne.keipert@helmholtz-muenchen.de).

panied by an increased browning and substantially increased respiratory capacity of WAT depots.

MATERIALS AND METHODS

Animals. UCP1-transgenic (UCP1-Tg) animals were generated as described previously (38). Experiments were performed in adult male hemizygous UCP1-Tg and their wild-type (WT) littermates. Mice were housed in groups with ad libitum access to food and water at 23°C and a 12:12-h dark-light cycle. From 12 wk of age, mice were fed a low-fat diet (LFD) or a high-fat diet (HFD) (32) for 8 or 30 wk. Unless otherwise stated, all data are from adult male mice of ~20 wk of age. Animal maintenance and experiments were approved by the ethics committee of the Ministry of Agriculture and Environment (State of Brandenburg, Germany; permission no. GZ 23-2347-8-2009).

Body composition and bone mineral density. Body composition was determined by quantitative magnetic resonance (Bruker's Minispec MQ10, Houston, TX), and bone mineral density was determined by dual-energy X-ray absorptiometry (Lunar Piximus).

Gene expression analysis. RNA isolation and quantitative real-time PCR (qPCR) were performed as described before (33). Quadriceps and gastrocnemius combined were used for analysis of SM gene expression. Multitissue gene expression was calculated as ΔC_T, using β-actin for normalization. Tissue-specific gene expression was calculated as $\Delta\Delta C_T$, using β-actin or β2 microglobulin (B2M) for normalization and relative to the WT group, which was normalized to a value of 1. The oligonucleotide primer (probe) sequences are listed in Table 1.

Growth factor analysis. FGF21 (mouse/rat FGF21 Quantikine ELISA Kit; R & D Systems), GH (rat/mouse growth hormone ELISA; Millipore), and IGF-I (mouse/rat IGF-I Quantikine ELISA Kit; R & D Systems) values were determined by ELISA, following the manufacturers' instructions.

Citrate synthase and cytochrome c oxidase activity assay. Citrate synthase (CS) activity was determined spectrometrically, as described previously (55), by monitoring the formation of DTNB at 412 nm. Briefly, muscle tissue was homogenized in 50 mM Tris, 1 mM EDTA (pH 7.4), and 0.1% Triton X-100 and centrifuged at 13,000 *g* for 10 min at 4°C. The supernatant was used to determine the protein content and CS activity levels. Ten microliters of 1:6 diluted tissue extract was loaded into one well of a 96-well plate. Afterward, 215 μl of reaction buffer [100 mM Tris, 1 mM $MgCl_2$, 1 mM EDTA (pH 8.2), and 0.1 M DTNB] and 25 μl of acetyl-CoA (3.6 mM) were added. All analyses were completed in triplicate. To start the reaction, 50 μl of oxaloacetate (3 mM) was added, and the absorbance change at 412 nm was measured for 10 min at 37°C. The CS activity was calculated from the slope of the linear portion of the absorbance curve.

Cytochrome *c* oxidase (COX) activity was determined as described previously (44), with slight modifications by recording oxygen consumption with an OROBOROS Oxygraph-2k. Subcutaneous WAT was homogenized in tissue buffer [10 mM HEPES, 40 mM KCl, 2 mM EGTA, 1% (vol/vol) Tween-20, 2 μM PMSF, and 10 mM Kaliumfluorid] with a Potter-type homogenizer and afterward sonicated with several short bursts. The homogenate was used to determine the protein content and COX activity levels in the tissues. The assay buffer contains 50 mM KH_2PO_4, 2 mM EGTA, 10 mM ascorbic acid, 5 mM ADP, and 2 μM oligomycin, and the reaction was started by the addition of cytochrome *c* (final concentration of 40 μM). Finally, COX activity was determined by recording oxygen consumption
at 37°C.

Histology. WAT and SM were fixed in 4% formaldehyde, embedded in paraffin, and cut into 2-μm slices. Hematoxylin and eosin (H & E) staining (Roth, Fluka) was performed to visualize nuclear and cytoplasmic sections within the cell. Quantification of cross-sectional area was performed using Adiposoft (1.0; Center for Applied Medical Research of the University of Navarra, Spain) (5).

Immunoblotting. Protein was prepared from frozen skeletal muscle (quadriceps and gastrocnemius combined), liver, and subcutaneous WAT (sWAT). Protein isolation, immunoblotting, and detection were performed as described previously (33). Immunoblots were performed using FGF21 and KLB antibody (R & D Systems), SQSTM1/p62 antibody (PROGEN Biotechnik), phosphorylated acetyl-CoA carboxylase (p-ACC)1 (Ser^{79}), p-ACC2 (Ser^{221}), ACC1/2, activating transcription factor 4 (ATF4), beclin-1, autophagy-related protein 7 (ATG7), phosphorylated eukaryotic initiation factor-2α (p-eIF2α; Ser^{51}), eIF2α, p-ERK1/2 ($Thr^{202/204}$), ERK1/2, fatty acid synthase (FASN), phosphorylated hormone-sensitive lipase (p-HSL; Ser^{660}), HSL, and LC3I/II (LC3B) antibodies (Cell Signaling Technology), OXPHOS antibody (MitoSciences/Abcam) and UCP1, and PCK1 antibodies (Abcam). GLUT1 antibody was kindly provided by Annette Schuermann (Department of Experimental Diabetology, Potsdam-Rehbruecke, Germany). Protein expression was normalized to α-tubulin (Sigma).

Ex vivo SM culture and cell culture. Ex vivo SM culture was adapted to a protocol described previously (33). Briefly, mice were fasted for 4 h prior the dissection of muscles. Mice were euthanized under isoflurane anesthesia. Extensor digitorum longus (EDL) and soleus muscles were rapidly removed, washed, and incubated in preoxygenated (95% O_2-5% CO_2) Krebs-Henseleit buffer (KHB) supplemented with 15 mM mannitol and 5 mM glucose for 2 h at 30°C in a humidified incubator containing 5% CO_2. Subsequently, muscles were washed in KHB, snap-frozen in liquid nitrogen, and stored at −80°C. Conditioned medium was centrifuged, and supernatant was stored at −20°C until analysis. C_2C_{12} cells were cultured in DMEM supplemented with 10% FBS and 1% penicillin-streptomycin at 37°C in a 5% CO_2 atmosphere. When C_2C_{12} cells reached 90% confluence, differentiation was induced by incubation for 6 days, with DMEM containing 2% horse serum and 1% penicillin-streptomycin. For RNA or protein isolation, the differentiated C_2C_{12} muscle cells were treated with 0 (control), 0.5, 5, or 10 μM FCCP (Sigma) for 24 h or with 4 μM antimycin A (Sigma) and 4 μM myxothiazol (Sigma) for 8 h (n = 3–5 biological replicates).

Murine WAT cell culture, differentiation, and treatment. The subcutaneous WAT pads of five WT mice (7 wk old) were dissected, minced, and digested [50 min at 37°C at 100 rpm in DMEM-F-12 plus glutamax containing 0.15% collagenase type IV (Life Technologies) and 2% BSA]. The digested tissue was then filtered through a 100-μm cell strainer and centrifuged at 400 *g* for 10 min to pellet the stromal vascular (SV) fraction. The SV cells were then resuspended in erythrocytes-lysis buffer (154 mM NH_4Cl, 10 mM $KHCO_3$, and 0.1 mM EDTA), incubated for 20 min at room temperature, and centrifuged at 400 *g* for 10 min. SV cells were resuspended in growth medium (DMEM-F-12 plus glutamax, 1% penicillin-streptomycin, and 10% FBS) and again filtered through a 40-μm cell strainer and plated on a T75 flask. For differentiation, SV cells were plated in 12-well plates, allowing them to grow to 90–100% confluence. At confluence, differentiation was started using a white fat differentiation cocktail as described previously (19) containing growth medium with 1 μM dexamethasone, 0.5 mM isobutylmethylxanthine, 5 μg/ml insulin, and 1 μM rosiglitazone. On *day 3* of differentiation, cells were exposed to DMEM-F-12 plus glutamax, 1% penicillin-streptomycin, 5 μg/ml insulin, and 20% WT or UCP1-Tg serum both with and without 2 μg of mouse FGF21 antibody (R & D Systems) for another 5 days (with 1 culture medium change after 3 days). On *day 7* of differentiation, cells were harvested, and RNA was isolated (Qiagen-RNeasy Lipid Tissue Kit) for gene expression analyses.

Statistical analysis. Statistical analyses were performed using Graph Prism (5.0) (GraphPad, San Diego, CA). Data are reported as means ± SE. Two-tailed Student's *t*-test was used to determine differences between the genotype. One-way ANOVA was used to

Table 1. *Oligonucleotide primer sequences*

Gene	Gene ID	PCR Primers
β-Actin	ACTB	Forward: TGT TAC CAA CTG GGA CGA CA Reverse: GGG GTG TTG AAG GTC TGA AA Probe: ACC GTG AAA AGA TGA CCC AG
Acetyl-coenzyme A carboxylase-α	ACACA	Forward: TTT CAC TGT GGC TTC TCC AG Reverse: TGC TAA TCA CTG CTG CAA TA Probe: CCA TTG TTG GCG ATA AGA ACC TTC TCA
Patatin-like phospholipase domain containing 2	PNPLA2	Forward: AAC AAC AGC ATC CAG TTC AA Reverse: GGT TCA GTA GGC CAT TCC TC Probe: CGA AGG CTC TCT TCC CGC CA
Fatty acid synthase	FASN	Forward: TTG ATG ATT CAG GGA GTG GA Reverse: TTA CAC CTT GCT CCT TGC TG Probe: CAT AGA CCC GCC GAG CCA GG
Hormone-sensitive lipase	LIPE	Forward: GCT TGG TTC AAC TGG AGA GC Reverse: TGC CTC TGT CCC TGA ATA GG Probe: CTG CTG CCC GAA GGG ACA CA
Phospho*enol*pyruvate carboxykinase 1	PEPCK1	Forward: TTT GTA GGA GCA GCC ATG AG Reverse: TGA TGA TCT TGC CCT TGT GT Probe: CTG CAG CAG CTG TGG CCT CA
Peroxisome proliferator-activated receptor-α	PPARA	Forward: ATT CGG CTG AAG CTG GTG TA Reverse: AAG CGA ATT GCA TTG TGT GA Probe: CGA CAA GTG TGA TCG GAG CTG CA
Peroxisome proliferator-activated receptor-γ	PPARG	Forward: TGC CAA AAA TAT CCC TGG TT Reverse: GGC GGT CTC CAC TGA GAA TA Probe: ACA CGA TGC TGG CCT CCC TG
Peroxisome proliferator-activated receptor-γ coactivator-1α	PPARGC1A	Forward: CTA CAG ACA CCG CAC ACA CC Reverse: GCG CTC TTC AAT TGC TTT CT Probe: CCC GCT TCT CGT GCT CTT TGC
Uncoupling protein 1	UCP1	Forward: AGT ACC CAA GCG TAC CAA GC Reverse: AGA AGC CAC AAA CCC TTT GA Probe: AAG GCC GTC GGT CCT TCC TTG
β-Actin	ACTB	Forward: GCC AAC CGT GAA AAG AGA C Reverse: TAC GAC CAG AGG CAT ACA G
Acetyl-coenzyme A carboxylase-β	ACACB	Forward: GCC TCT TCA TCA CCA ACG AG Reverse: AAA GAG AGC CTG CCT GAA CA
Activating transcription factor 4	ATF4	Forward: GGA ATG GCC GGC TAT GG Reverse: TCC CGG AAA AGG CAT CCT
Activating transcription factor 5	ATF5	Forward: CTA CCC CTC CAT TCC ACT TTC C Reverse: TTC TTG ACT GGC TTC TCA CTT GTG
Activating transcription factor 6	ATF6	Forward: CTT CCT CCA GTT GCT CCA TC Reverse: CAA CTC CTC AGG AAA CGT CT
β2-microglobulin	B2M	Forward: CCC CAC TGA GAC TGA TAC ATA CGC Reverse: AGA AAC TGG ATT TGT AAT TAA GCA GGT TC
Cell death-inducing DNA fragmentation factor, α-subunit-like effector A	CIDEA	Forward: TGC TCT TCT GTA TCG CCC AGT Reverse: GCC GTG TTA AGG AAT CTG CTG
DNA-damage inducible transcript 3	DDIT3	Forward: AGA GTG GTC AGT GCG CAG C Reverse: CTC ATT CTC CTG CTC CTT CTC C
Fibroblast growth factor 21	FGF21	Forward: GCT GCT GGA GGA CGG TTA CA Reverse: CAC AGG TCC CCA GGA TGT TG
Fibroblast growth factor receptor 1	FGFR1	Forward: TGT TTG ACC GGA TCT ACA CAC A Reverse: CTCCCACAAGAGCACTCCAA
Fibroblast growth factor receptor 2	FGFR2	Forward: TCG CAT TGG AGG CTA TAA GG Reverse: CGG GAC CAC ACT TTC CAT AA
Fibronectin type III domain-containing 5	FNDC5	Forward: ATG AAG GAG ATG GGG AGG AA Reverse: GCG GCA GAA GAG AGC TAT AAC A
Protein phosphatase 1 regulatory (inhibitor) subunit 15A	PPP1R15a	Forward: GTC CAT TTC CTT GCT GTC TG Reverse: AAGGCGTGTCCATGCTCTGG
Interleukin-15	IL-15	Forward: CTC AGA GAG GTC AGG AAA GAA TCC Reverse: GAC CAT GAA GAG GCA GTG CTT
Interleukin-6	IL-6	Forward: TAG TCC TTC CTA CCC CAA TTT CC Reverse: TTG GTC CTT AGC CAC TCC TTC
β-Klotho	KLB	Forward: GAT GAA GAA TTT CCT AAA CCA GGT T Reverse: AAC CAA ACA CGC GGA TTT C
Leucine-rich α2-glycoprotein 1	LRG1	Forward: CCT CAA GGA ATG CCT GAT ACT G Reverse: TTG GAG AAT TCC ACC GAC AG
Tissue inhibitor of metalloproteinase 4	TIMP4	Forward: GAC CCT GCT GAC ACT CAA AAA C Reverse: GGA AGA GTC AAA TGG CGT GTA G
Uncoupling protein 1 (native)	native UCP1	Forward: CGT GCC CGC ATC AGG CAA CA Reverse: TTG GAG GGC AGA GAG GCG TGA
Vascular endothelial growth factor-β	VEGFB	Forward: TAT CTC CCA GAG CTG CCA TCT A Reverse: GCC AGA AGA TGC TCA CTT GAC

evaluate differences between groups with appropriate post hoc tests. Statistical significance was assumed at $P < 0.05$.

RESULTS

FGF21 expression and increased secretion from SM in UCP1-Tg mice. Real-time RT-PCR gene expression analysis of relevant myokines (Fig. 1*A*) showed a massive increase of FGF21 in SM of UCP1-Tg mice compared with WT mice. Of the other myokines investigated, only vascular endothelial growth factor-B and interleukin 6 (IL-6) showed significant but much lower increased expression in UCP1-Tg muscle. FGF21 is considered to be preferentially expressed in liver (51), but it is also found in other metabolic tissues such as WAT and BAT (47). We examined FGF21 gene expression in several metabolic tissues in WT mice and observed that it was highest in liver and much lower in inguinal subcutaneous WAT (sWAT) and SM (Fig. 1*B*). We also confirmed that the induction of FGF21 in UCP1-Tg mice was specific to SM, whereas FGF21 mRNA was ~50-fold higher than in liver (Fig. 1*B*).

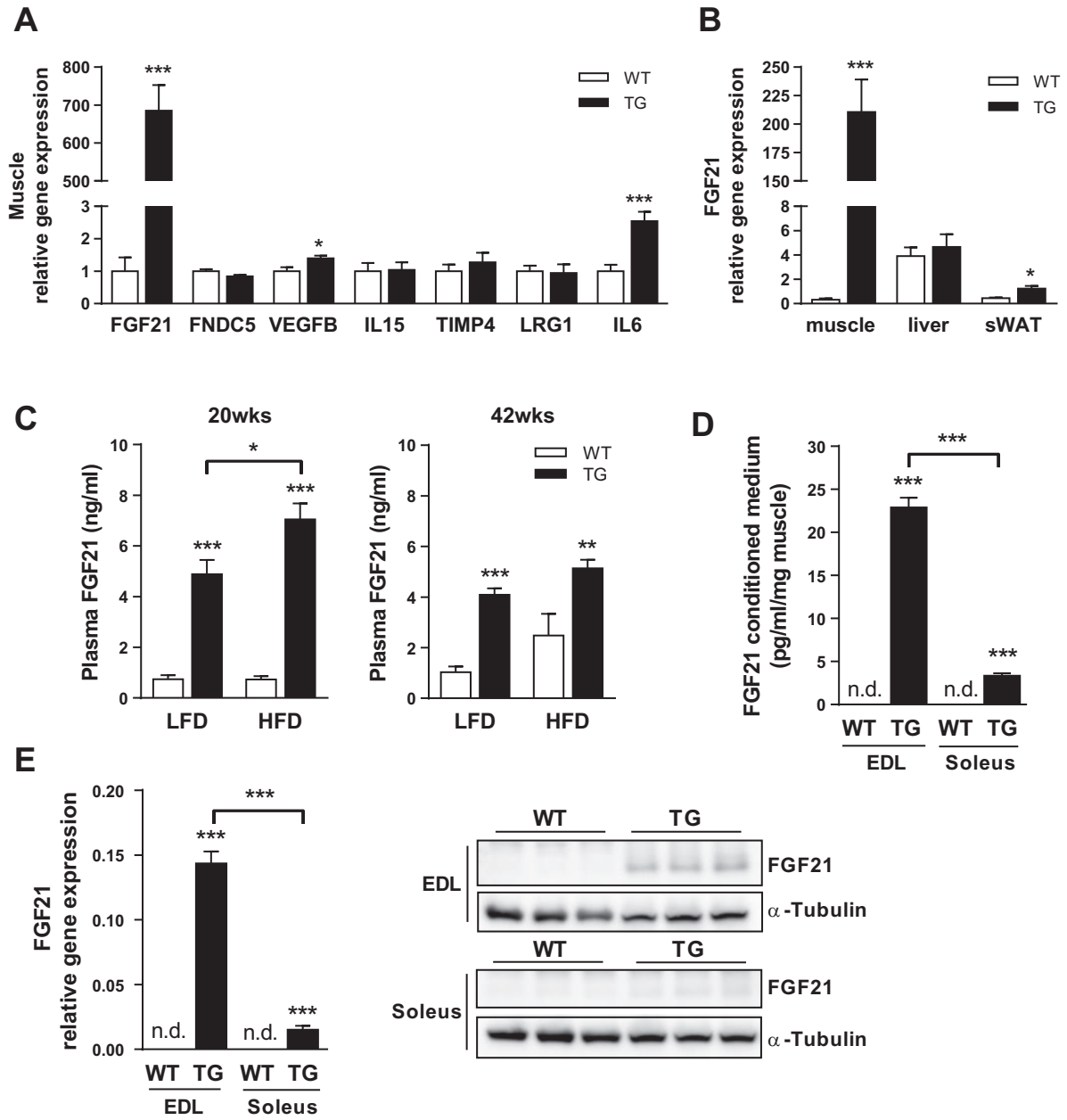

Fig. 1. Fibroblast growth factor 21 (FGF21) expression and increased secretion from skeletal muscle (SM) in uncoupling protein 1-transgenic (UCP1-Tg) mice. *A* and *B*: quantitative PCR (qPCR) analysis of myokines in SM (*A*) and FGF21 in SM, liver, and subcutaneous WAT (sWAT) of wild-type (WT) and UCP1-Tg mice (*B*). *C*: plasma FGF21 concentration of WT and UCP1-Tg mice fed a low-fat diet (LFD) or high-fat diet (HFD) since 12 wk of age in mice aged 20 (*left*) and 42 wk (*right*). *D*: ex vivo secretion of FGF21 (pg/ml) from extensor digitorum longus (EDL) or soleus muscle of WT and UCP1-Tg mice after 2-h incubation normalized to muscle wet weight (mg). *E*: gene expression and representative immunoblots of EDL or soleus muscle from WT and UCP1-Tg mice (α-tubulin was used as a control). $^{*}P < 0.05$, $^{**}P < 0.01$, and $^{***}P < 0.0001$, significant differences between the genotypes; $n = 6–8$/group. ND, not detectable. Data are means ± SE. FNDC, fibronectin type III domain-containing 5; LRG1, leucine-rich α2-glycoprotein 1; TIMP4, tissue inhibitor of metalloproteinase 4.

Analysis of plasma FGF21 levels showed around fivefold increased plasma levels in UCP1-Tg mice compared with WT mice and was in the range of 5–7 ng/ml (Fig. 1*C*). This is slightly higher than previously reported fasting levels in mice but lower than plasma levels of FGF21 transgenic mice, which were ~20 ng/ml (29). We further investigated the effect of age and diet on FGF21 plasma levels of mice fed HFD or LFD until they reached the age of 20 (Fig. 1*C*, *left*) or 42 wk (Fig. 1*C*, *right*). In a previous study (33), we could show that WT mice developed obesity accompanied by increased liver triglycerides and elevated plasma insulin levels already at 20 wk. UCP1-Tg mice were not affected by HFD at 20 wk but became obese in older age. Interestingly, young UCP1-Tg mice showed highly increased FGF21 plasma levels compared with WT on both diets, being even higher on the HFD (Fig. 1*C*). In older age (42 wk), FGF21 plasma levels decreased slightly in UCP1-Tg mice. In young WT mice there was no effect of diet on FGF21 plasma levels, but it was elevated (albeit not significantly) by HFD feeding in older mice. The increased FGF21 levels on HFD agree with increased circulating FGF21 in obesity in different mouse models and humans (27). This is linked to a FGF21 resistance, evidenced by a large attenuation of FGF21 effects on liver and adipocytes (17) due possibly to an inflammation-induced repression of KLB expression, as shown in adipocytes (13).

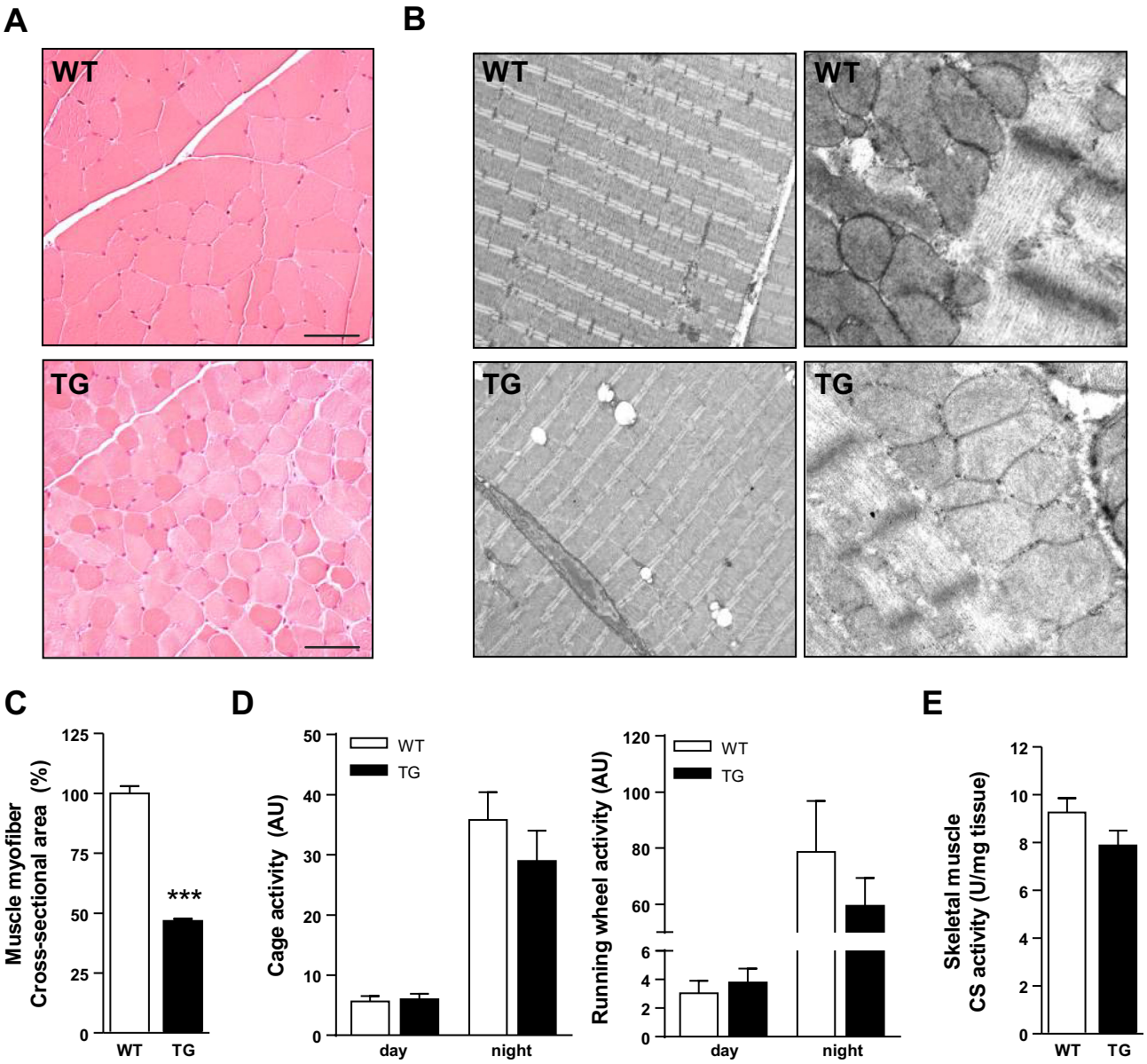

Fig. 2. Reduced muscle mass without muscle dysfunction or features of myopathy in UCP1-Tg mice. *A*: representative hematoxylin and eosin staining of tibialis muscle from a WT and a UCP1-Tg mouse showing a general decrease in myofiber size but no different features of muscle degeneration, including central nuclei and vacuolated fibers. Scale bars, 50 μm. *B*: representative electron micrographs of WT and UCP1-Tg gastrocnemius muscles. *C*: quantification of cross-sectional area of myofibers; data from 3 mice in each group. *D*: locomotor activity [normal cage activity (*left*) and voluntary running wheel activity (*right*)] of WT and UCP1-Tg mice. *E*: citrate synthase (CS) activity in SM. ***$P < 0.0001$, significant differences between the genotypes; $n = 5–8$/group. Data are means ± SE.

Moreover, secretion of FGF21 from SM was confirmed by 2-h ex vivo incubation of isolated SM (Fig. 1*D*). FGF21 concentrations were below the detection limit in medium from WT muscles but were very substantial in both soleus and EDL muscles from UCP1-Tg mice. FGF21 secretion was around sixfold higher in EDL, a fast-twitch, glycolytic type II muscle, than in soleus, a slow-twitch, oxidative, type I muscle. We detect the same pattern in FGF21 gene and protein expression, with higher expression in EDL compared with soleus muscle (Fig. 1*E*). This agrees with protection from the uncoupling effects of UCP1 of slow-twitch muscles because of their high continuous ATP synthesis (9) and suggests that the induction of FGF21 expression in SM is tightly linked to the actual mitochondrial uncoupling induced by UCP1.

Reduced muscle mass without muscle dysfunction or features of myopathy in UCP1-Tg mice. Until now, a possible contribution of muscle FGF21 secretion to circulating FGF21 was shown only in models of mitochondrial dysfunction and myopathy (37, 59). Therefore, we investigated in more detail UCP1-Tg muscle physiology and morphology. Histology showed reduced fiber size but no apparent degenerative changes in SM morphology, such as central nuclei (Fig. 2, *A* and *C*), misalignment of Z-line, or abnormal mitochondria (Fig. 2*B*). This is in line with previous findings, where we could show that there is no evidence for alterations in mitochondrial function and density despite a decreased muscle mass in UCP1-Tg mice compared with WT littermates (33). Physiological muscle function was also not impaired, as evident from recordings of normal cage activity (using infrared sensors) as well as voluntary running wheel activity. Both showed no differences between UCP1-Tg and WT mice (Fig. 2*D*). Furthermore, we also measured SM CS activity as a marker for mitochondrial density and could detect no differences between UCP1-Tg and WT mice (Fig. 2*E*).

No basal autophagy defect in muscle of UCP1-Tg mice. Autophagy is required for maintenance of normal muscle function (53), and suppression of SM autophagic flux was shown to lead to severe muscle dystrophy and mitochondrial dysfunction but also to an induction of FGF21 expression and release from muscle (37). Here, we assessed basal autophagy as nonstimulated autophagic flux by measuring protein levels of LC3-I (microtubule-associated protein 1 light chain 3-MAP1LC3A or LC3) and LC3-II (which is the phosphatidylethanolamine-conjugated and by this activated form of LC3-I) and the LC3-II/LC3-I ratio as marker of LC3-I to LC3-II conversion as well as the protein content of sequestosome 1 (SQSTM1 or p62) (31, 45, 46). p62 is one of the best characterized substrates of selective autophagy, which is incorporated via direct interaction with LC3 into the autophagosome and by this degraded during the autophagic process (30, 61). It is important to highlight that impairment of autophagy is accompanied by an accumulation of p62, as also observed in muscle-specific ATG7-knockout mice (37, 39). Therefore, we further analyzed the protein expression levels of BECLIN-1 and ATG7 as additional key proteins that are involved in autophagosome formation (25, 43). UCP1-Tg muscle showed elevated LC3-II protein levels, but without increased LC3-II/LC3-I ratio and a trend of reduced p62 protein content ($P = 0.06$) compared with WT littermates (Fig. 3, *A* and *B*). Moreover, total LC3 (LC3-I + LC3-II), BECLIN-1, and ATG7 protein expression were increased in muscle of UCP1-Tg mice (Fig. 3, *A* and *C*). This is indicative for an induction of autophagic machinery, but without increased basal autophagy flux. However, these results clearly show that, in contrast to

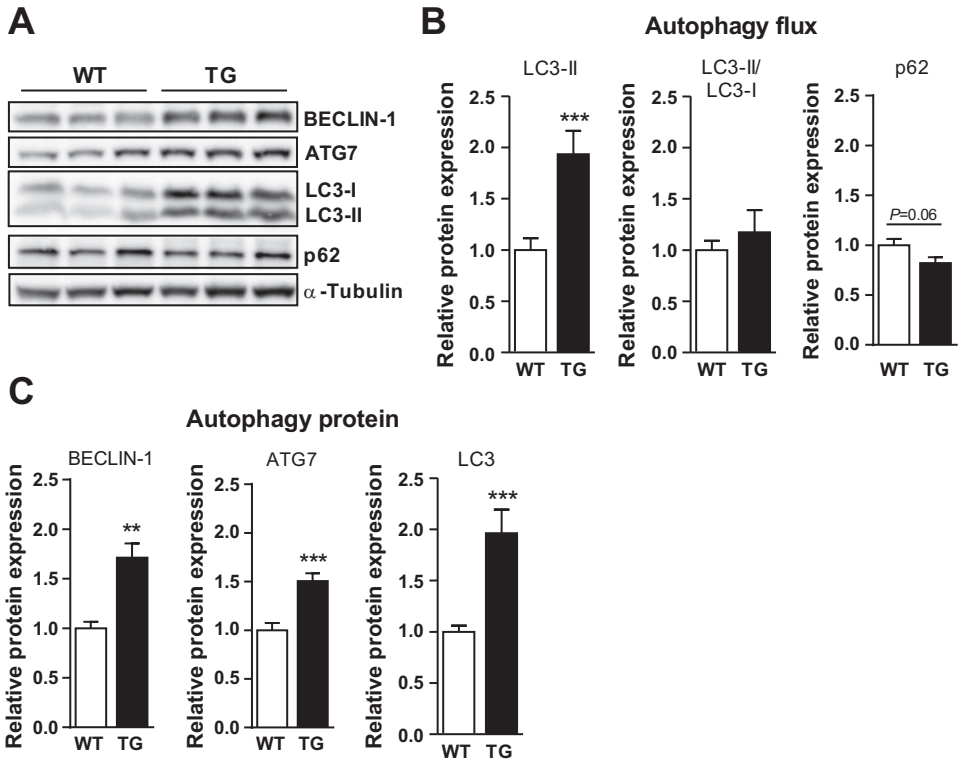

Fig. 3. No basal autophagy defect in muscle of UCP1-Tg mice. *A*: representative immunoblots of key proteins involved in autophagy from SM of WT and UCP1-Tg mice. *B*: quantification of LC3-II, LC3-II/LC3-I ratio, and p62 protein collectively as markers of basal autophagy flux. *C*: quantification of BECLIN-1, autophagy-related protein 7 (ATG7), and total LC3 (LC3-I + LC3-II) proteins (α-tubulin was used as a control). $^{**}P < 0.01$ and $^{***}P < 0.0001$, significant differences between the genotypes; $n = 6$/group. Data are means ± SE.

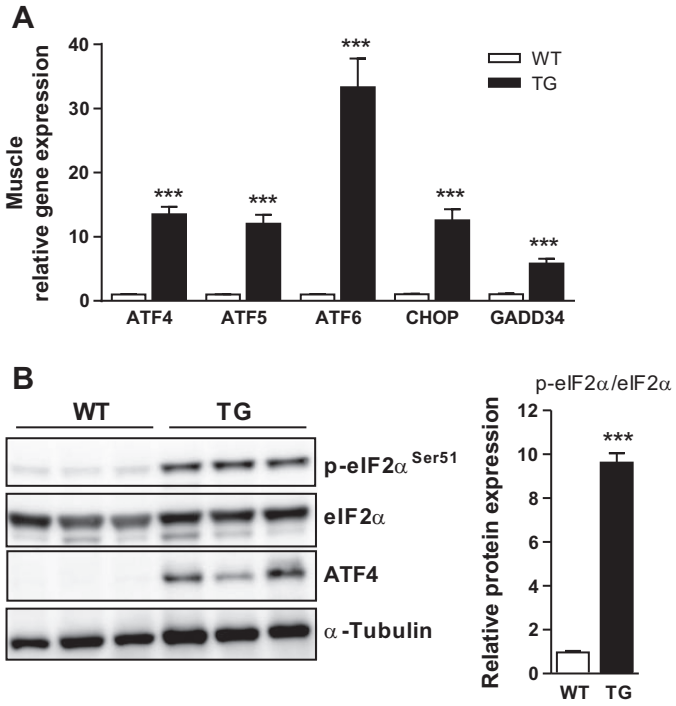

Fig. 4. Activation of integrated stress response (ISR) in muscle of UCP1-Tg mice. *A*: qPCR analysis of ISR-related genes in SM of WT and UCP1-Tg mice. *B*: representative immunoblots and quantification of total (eIF2α) and phosphorylated (p-eIF2α) eukaryotic initiation factor-2α and activating transcription factor 4 (ATF4) protein in skeletal muscle of WT and UCP1-Tg mice (α-tubulin was used as a control). ***$P < 0.0001$, significant differences between the genotypes; $n = 6–8$/group. Data are means ± SE. CHOP, CCAAT/enhancer-binding protein homologous protein; GADD34, growth arrest and DNA damage-inducible protein 34.

Kim et al. (37), our mouse model has no signs of autophagy deficiency.

Activation of integrated stress response in muscle of UCP1-Tg mice. Although overall SM function is preserved in UCP1-Tg mice, we have previously found evidence for an increased cellular stress (33). Recent studies (37) have implicated the eIF2α/ATF4 cascade, which is part of the integrated stress response (ISR), in the induction of FGF21 gene expression in muscle. Real-time RT-PCR analysis showed highly increased expression of genes related to the ISR pathway in SM of UCP1-Tg mice (Fig. 4*A*). This included not only ATF4 but also ATF5 and ATF6 together with an increased expression of DNA damage-inducible transcript 3 (DDIT3 or CCAAT/enhancer-binding protein homologous protein) and protein phosphatase 1 regulatory (inhibitor) subunit 15A (PPP1R15a or growth arrest and DNA damage-inducible protein 34), both of which are stress response genes known to be induced by ATF4 (42). Phosphorylation of eIF2α was highly increased in UCP1-Tg mice compared with WT mice (Fig. 4*B*), leading to the subsequent induction of ATF4 expression (Fig. 4, *A* and *B*). Both ATF4 and ATF5 are known downstream targets of eIF2α (64) and have been found to be involved in the induction of FGF21 gene expression in muscle (37, 59). Thus, these data link increased cellular stress, collectively an increased ISR, to FGF21 secretion in SM, demonstrating its role as a novel homeostatic response to increased SM stress.

Altered mitochondrial respiration induces FGF21 in muscle cells. To examine the cellular mechanisms leading to FGF21 induction in more detail, we treated differentiated C_2C_{12} cells with different compounds targeting mitochondrial function. This included the complex 3 inhibitors antimycin A and myxothiazol as well as the chemical uncoupler carbonyl cyanide 4 (trifluoromethoxy) phenylhydrazone (FCCP).

It is known that antimycin A, an inhibitor acting at the quinone reducing center (Qi), stimulates superoxide formation by inhibiting semiquinone oxidation, whereas myxothiazol, an inhibitor of the Qo site, inhibits superoxide production by preventing semiquinone formation (10, 58). Indeed, both mitochondrial stressors induced FGF21 gene expression in C_2C_{12} cells (Fig. 5*A*), suggesting that FGF21 expression is activated in response to mitochondrial stress independent of reactive oxygen species (ROS) production. To determine whether uncoupling of the respiratory chain itself can lead to an induction of FGF21 gene expression in vitro, we furthermore treated differentiated C_2C_{12} cells with the chemical uncoupler FCCP. C_2C_{12} cells treated with different concentrations of FCCP for 24 h showed a dose-dependent increase in FGF21 gene expression (Fig. 5*B*). The induction of FGF21 was also confirmed on protein levels (Fig. 5*C*). As in skeletal muscle of UCP1-Tg mice, in C_2C_{12} cells the increased FGF21 expression was associated with an activation of the eIF2α/ATF4 cascade

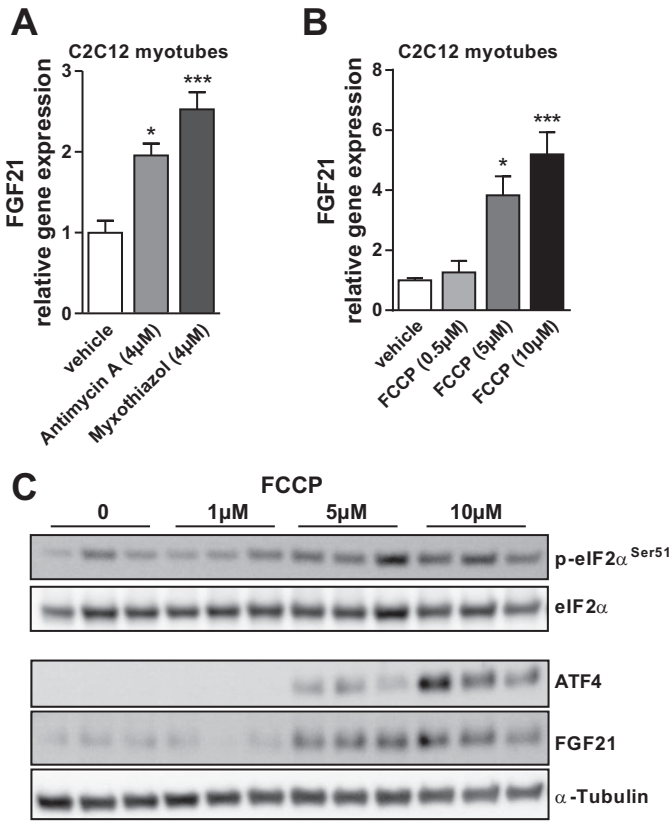

Fig. 5. Altered mitochondrial respiration induces FGF21 in muscle cells. *A* and *B*: qPCR analyses of FGF21 expression in C_2C_{12} myotubes treated for 8 h with antimycin A (4 μM) or myxothiazol (4 μM) (*A*) or for 24 h with the chemical uncoupler FCCP (*B*). *C*: representative immunoblots of p-eIF2α, total eIF2α, ATF4, and FGF21 after 24-h treatment with FCCP (α-tubulin was used as a control). *$P < 0.05$ and ***$P < 0.0001$, significant differences between the different concentrations; $n = 3$ (biological replicates). Data are means ± SE.

(Fig. 5*C*). These data clearly confirm that FGF21 acts as a myokine released from SM in response to an altered mitochondrial respiratory chain capacity and induced cellular stress response.

FGF21 receptors in potential target tissues. It has been suggested that FGF21 functions predominantly in a paracrine/autocrine manner because, so far, target tissues have also been the main tissues of FGF21 expression (35). However, the pronounced increase of circulating FGF21 in UCP1-Tg mice suggests possible endocrine actions. Therefore, we analyzed gene expression of FGF receptors FGFR1 and FGFR2 as well as the crucial coreceptor KLB in potential target organs. FGFR1 and FGFR2 (Fig. 6, *A* and *B*) showed opposite gene expression patterns throughout all tissues analyzed with FGFR1, showing very low expression levels in liver. In UCP1-Tg mice FGFR1 was downregulated, whereas FGFR2 was upregulated in liver. Gene expression of KLB was high in liver and sWAT and much lower in SM (Fig. 6*C*), whereas no differences in protein levels of KLB were detected in liver or sWAT, and no KLB protein expression at all was detected in SM (Fig. 6*D*). However, on gene expression level, KLB was increased in all tissues investigated in UCP1-Tg mice, suggesting a possible feedforward effect of FGF21 on its own signaling pathway.

Endocrine effects of skeletal muscle FGF21 on somatic growth and liver. FGF21 has been shown to inhibit GH signaling characterized by decreased levels of IGF-I and increased plasma levels of GH, which result in a reduced body size of mice overexpressing FGF21 (29). Furthermore, the FGF21-overexpressing mice display a reduced bone mass (60, 63). UCP1-Tg mice show a similar phenotype of reduced body length and lean body mass (32, 34) that was confirmed again in this study (Fig. 7*A*). Analysis of the GH/IGF-I axis showed significantly reduced circulating IGF-I levels in UCP1-Tg mice and increased GH levels (although they were not significant due to high variation; Fig. 7*B*). Additionally, they also showed a reduced bone mineral density (Fig. 7*C*). Most of the circulating IGF-I is produced in liver (62), and overall liver metabolism has been shown to be directly affected by FGF21 (18). Here, we found no differences in hepatic expression of genes related to lipid metabolism [peroxisome proliferator-activated receptor (PPAR)-γ and -α, acetyl-CoA carboxylase (α-ACACA, ACC1), and carnitine palmitoyltransferase 1α] between UCP1-Tg and WT mice, but we found an induction of PPARγ coactivator-1α (PGC-1α) and phospho*enol*pyruvate carboxykinase 1 (PEPCK1) gene expression (Fig. 7*D*), indicative of an increased gluconeogenesis rate and confirming previous findings with exogenous FGF21 application (17, 18). However, protein expression analysis of gluconeogenic markers (PEPCK1) and PGC-1α as well as phosphorylation of ACC1 and ACC2 (ACACB) as markers for the balance between fatty acid synthesis and fatty acid oxidation revealed no difference in liver of UCP1-Tg mice compared with WT (Fig. 7*E*). Therefore, we propose that, under standard diet conditions, liver substrate metabolism is not the main target of FGF21 secreted from uncoupled SM.

SM-secreted FGF21 leads to "browning" of WAT. WAT is an important target tissue of FGF21 action. Recently, FGF21 was found to induce the appearance of BAT-like adipocytes in WAT, with different depots showing various degrees of browning (19). UCP1-Tg mice show an increased glucose uptake (50) and an augmented lipid metabolism (32) in WAT. Also, as shown above, KLB is highly expressed in WAT. Therefore, we examined possible effects of FGF21 on different WAT depots, i.e., sWAT and epididymal WAT (eWAT) depots. Histology showed an altered morphology of both sWAT and eWAT from UCP1-Tg mice compared

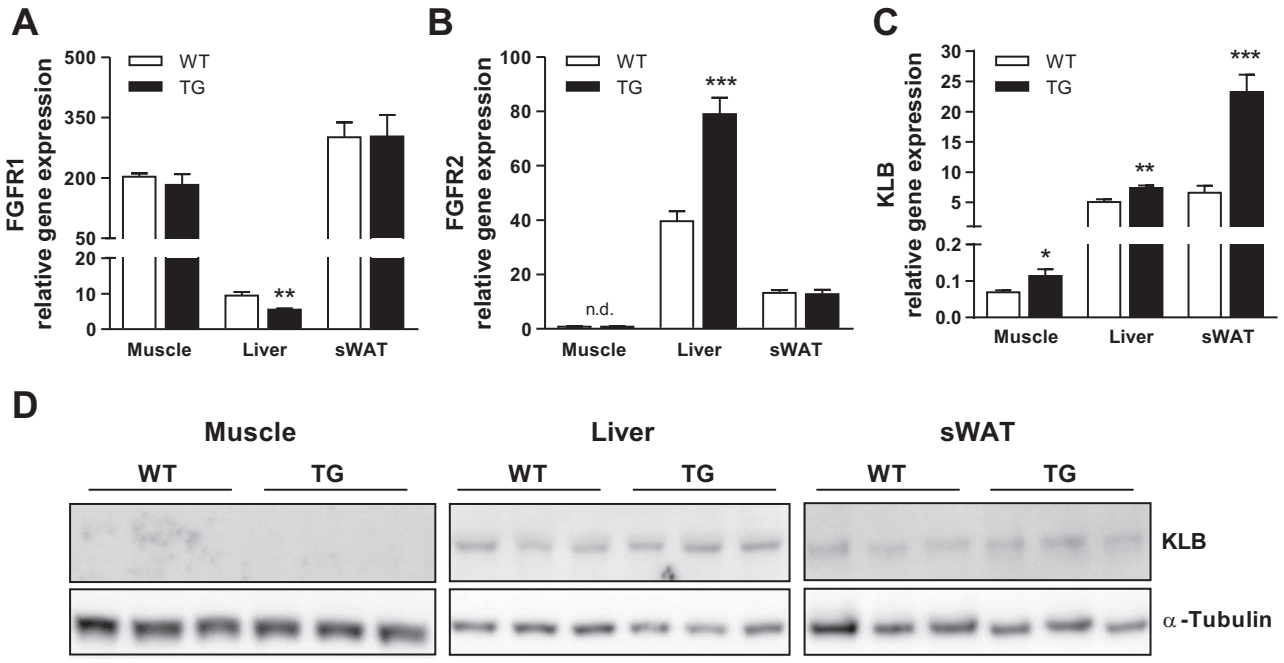

Fig. 6. FGF21 receptors in potential target tissues. *A–C*: qPCR analysis of FGF receptor (FGFR)1 (*A*), FGFR2 (*B*), and β-Klotho (KLB; *C*) in SM, liver, and sWAT of WT and UCP1-Tg mice. *D*: representative immunoblots of KLB protein expression in muscle, liver, and sWAT (α-tubulin was used as a control). $^{*}P < 0.05$, $^{**}P < 0.01$, and $^{***}P < 0.0001$, significant differences between the genotypes; $n = 6–10$/group. Data are means ± SE.

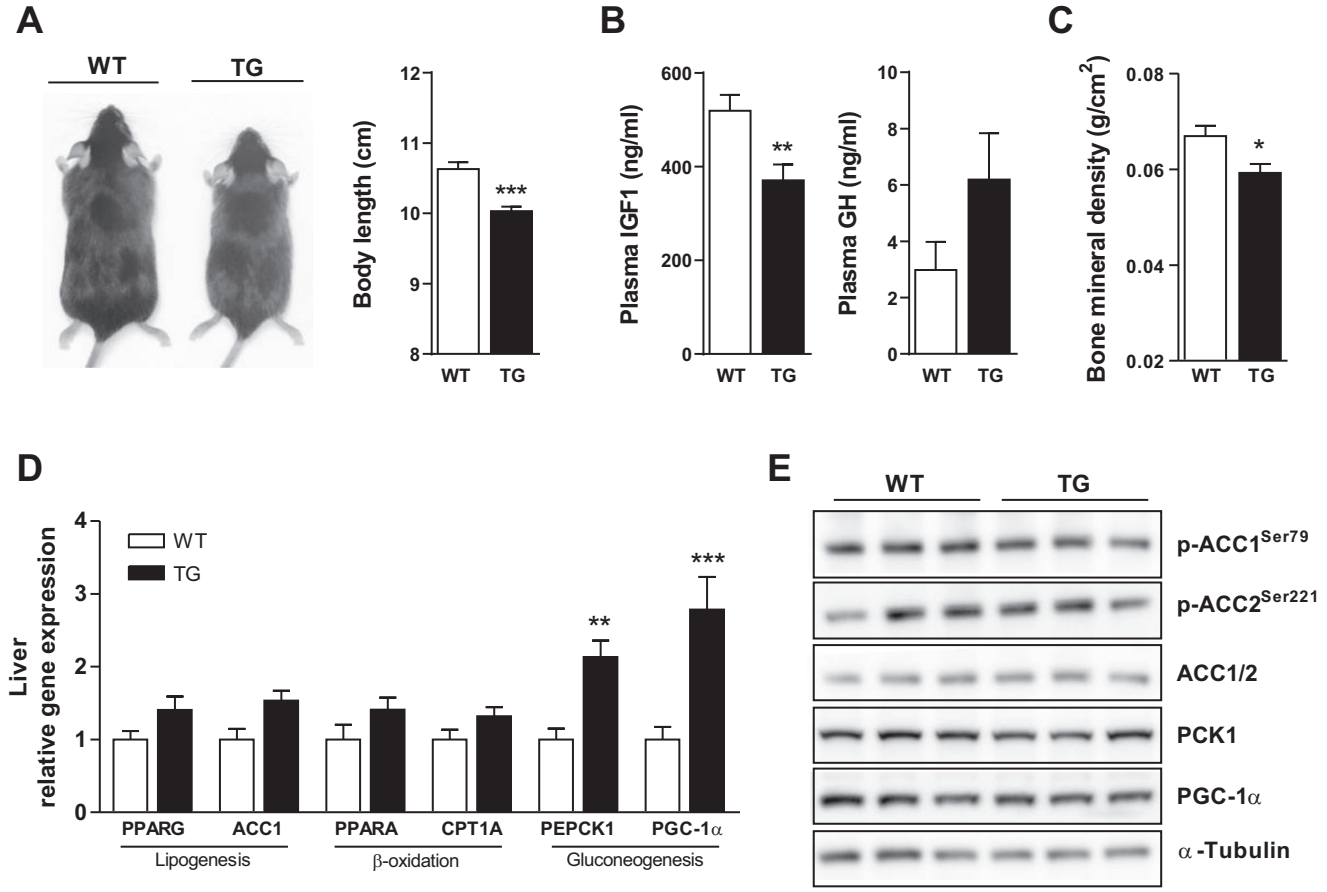

Fig. 7. Endocrine effects of skeletal muscle FGF21 on somatic growth and liver metabolism. *A*: representative image of a male adult WT and UCP1-Tg mouse and body length (nose tip to tail base) of WT and UCP1-Tg mice. *B*: analysis of growth hormone (GH)/insulin-like growth factor I (IGF-I) axis with plasma levels of IGF-I (*left*) and GH (*right*) in WT and UCP1-Tg mice. *C*: bone mineral density analyzed by dual-energy X-ray absorptiomery scan in WT and UCP1-Tg mice. *D*: qPCR analysis of liver gene expression in WT and UCP1-Tg mice. *E*: representative immunoblot image of phosphorylated acetyl-CoA carboxylase (p-ACC)1, p-ACC2, total ACC1/2, phospho*enol*pyruvate carboxykinase (PEPCK1), and PGC-1α (α-tubulin was used as a control) in liver. $*P < 0.05$, $**P < 0.01$, and $***P < 0.0001$, significant differences between the genotypes; $n = 6$–10/group. Data are means ± SE.

with WT, with more small, multilocular adipocytes present within fat depots of UCP1-Tg mice compared with WT mice (Fig. 8*A*). This was accompanied by an increased expression of typical BAT marker genes such as UCP1, CIDEA, and PGC-1α in sWAT and in eWAT (Fig. 8*B*). Subsequent analysis of protein expression in sWAT from UCP1-Tg mice showed an increased expression of enzymes of the respiratory chain (indicative of increased mitochondrial content) and increased UCP1 protein compared with WT (Fig. 8*C*). Furthermore, we measured COX activity as a functional marker for maximal mitochondrial respiratory capacity. Indeed, UCP1-Tg mice showed a highly significant, more than sevenfold increase of COX activity compared with WT mice (Fig. 8*D*). To ensure that overexpression of the transgenic UCP1 is indeed skeletal muscle specific and that the increased UCP1 gene expression in sWAT represents the native form of UCP1, we designed a primer pair that binds to the native but not to the transgenic (muscle-specific) UCP1 mRNA. We detected no native UCP1 expression in skeletal muscle, a high expression in BAT, and an induction in sWAT of UCP1-Tg mice compared with WT (Fig. 8*E*). This confirms that the increased expression of UCP1 in WAT of UCP1-Tg mice is due to a browning effect and not to a "leaky" expression of transgenic UCP1. To investigate whether the increased UCP1 expression in WAT depots of UCP1-Tg mice is linked directly to Tg muscle-secreted FGF21, we performed an in vitro study, adding 20% blood serum of WT or UCP1-Tg mice to murine primary white adipocytes with and without FGF21 antibody. Strikingly, in primary WAT treated with serum of UCP1-Tg mice, UCP1 gene expression was increased compared with WT serum treatment. In contrast, when adding serum of UCP1-Tg mice with FGF21 antibody to the incubation medium, no differences in UCP1 RNA levels between WT and UCP1-Tg mice were observed (Fig. 8*F*). These data demonstrate a skeletal muscle FGF21-induced "browning" linked to an increased oxidative capacity of WAT in UCP1-Tg mice.

Increased futile cycle but no effect on GLUT1 or ERK in WAT of UCP1-Tg mice. Because FGF21 also plays an important role in lipid metabolism (28), we had a closer look at mRNA levels of proteins related to lipogenesis (FASN and ACACA) as well as lipolysis (adipose triglyceride lipase and HSL). Interestingly, lipogenic as well as lipolytic genes were increased in both WAT depots of UCP1-Tg mice compared with WT (Fig. 9*A*), confirming an increased futile cycle of lipid storage and release, as reported before (32). Moreover, HSL

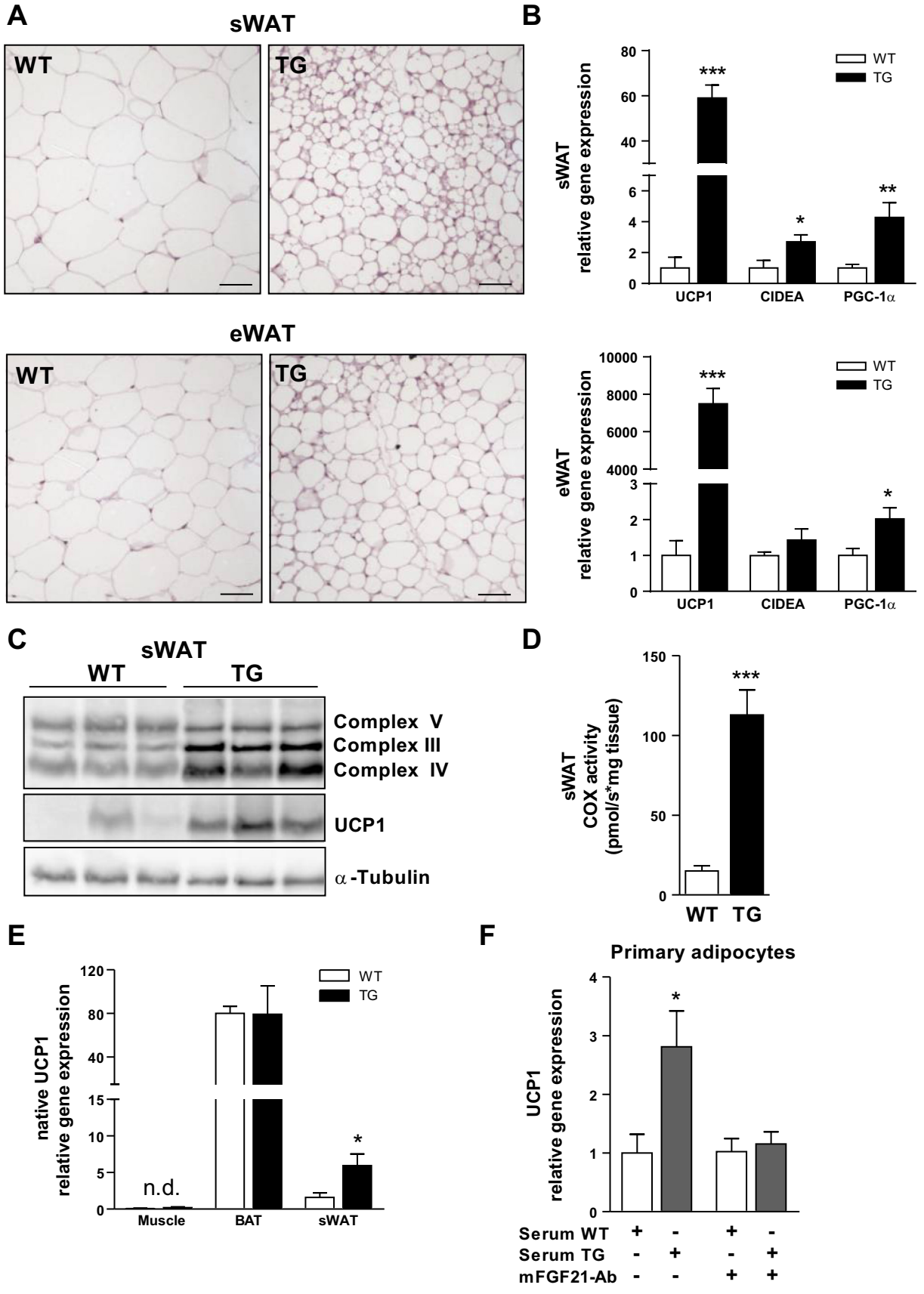
A
sWAT
WT
TG
eWAT
WT
TG
B
sWAT
relative gene expression
WT
TG
UCP1
CIDEA
PGC-1α
eWAT
relative gene expression
C
sWAT
WT
TG
Complex V
Complex III
Complex IV
UCP1
α-Tubulin
D
sWAT
COX activity
(pmol/s*mg tissue)
WT
TG
E
native UCP1
relative gene expression
n.d.
Muscle
BAT
sWAT
F
Primary adipocytes
UCP1
relative gene expression
Serum WT
Serum TG
mFGF21-Ab

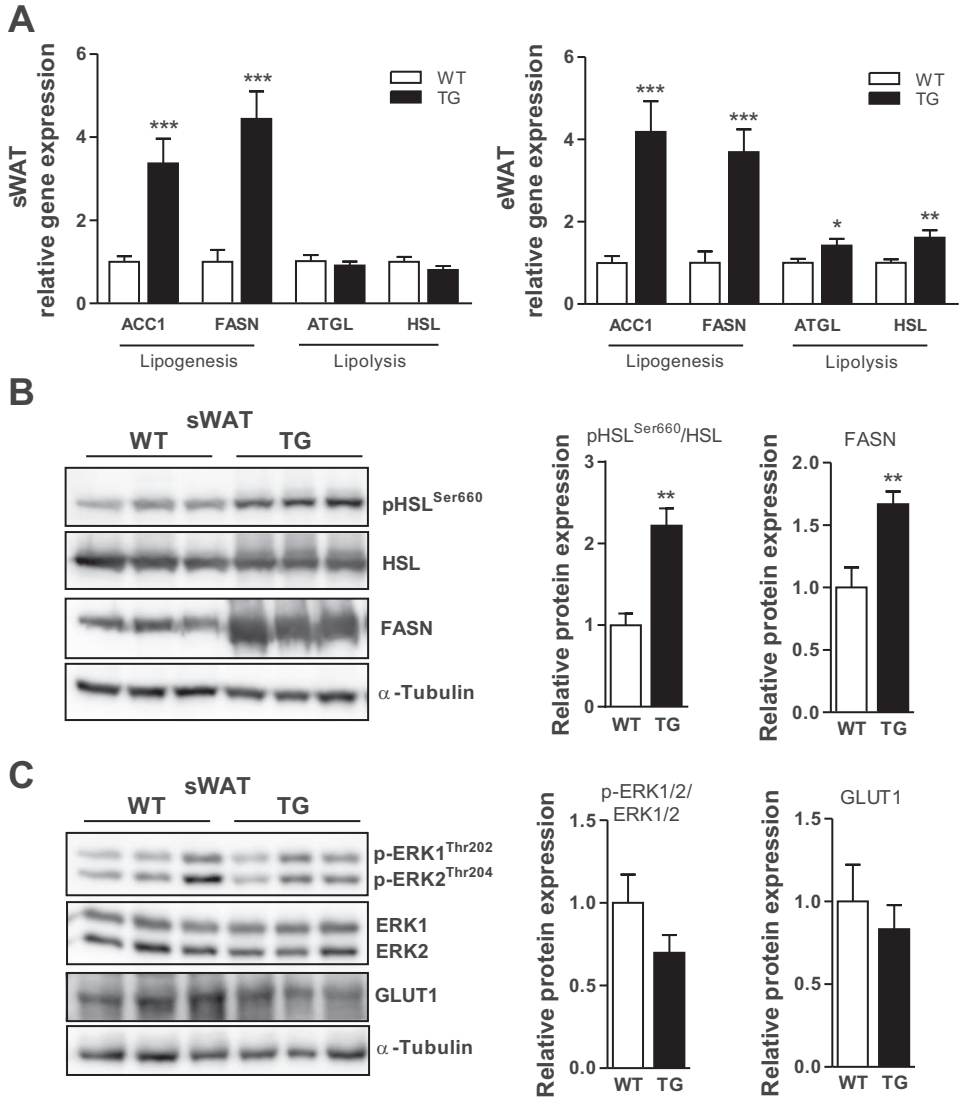

Fig. 9. Increased futile cycle but no effect on glucose transporter 1 (GLUT1) or ERK in WAT of UCP1-Tg mice. *A*: qPCR analysis of lipogenesis- and lipolysis-related genes in sWAT and eWAT of WT and UCP1-Tg mice. *B*: immunoblot and quantification of p-HSL/HSL (hormone-sensitive lipase) and FASN (fatty acid snynthase) in sWAT of WT and UCP1-Tg mice. *C*: immunoblot and quantification of p-ERK1/2/ERK1/2 and GLUT1 in sWAT of WT and UCP1-Tg mice (α-tubulin was used as a control). $*P < 0.05$, $**P < 0.01$, and $***P < 0.0001$, significant differences between the genotypes; $n = 6–8$/. group. Data are means ± SE. ATGL, adipose tissue triglyceride lipase.

was just recently identified as a direct FGF21 target in WAT (11). Performing further protein analysis in sWAT depots, we measured levels of the activating phosphorylation of HSL on Ser^{660}, which was significantly upregulated in UCP1-Tg mice (Fig. 9*B*). MAP kinase ERK (p42/44 MAPK or ERK1/2) and the glucose transporter 1 (SLC2A1 or GLUT1) have been found to further intracellular downstream signaling targets of FGF21 (23). Measurement of phosphorylated ERK1/2 in sWAT and GLUT1 showed no differences between the genotypes (Fig. 9*C*). Altogether, this is in line with recent findings showing that FGF21 induces lipolysis in WAT without induction of ERK1/2 signaling pathways (11).

DISCUSSION

Here, we show evidence that the improved metabolic phenotype of UCP1-Tg mice is linked to an induction of endocrine-acting FGF21 expression and secretion from skeletal muscle. FGF21 is considered mainly as a starvation signal secreted by liver, although it is expressed in other tissues such as adipose tissue, SM, testis, and pancreas (3, 15, 21, 35, 51, 57). Until now, evidence for a possible contribution of muscle FGF21 secretion to circulating FGF21 was restricted to models of mitochondrial myopathy (37, 56, 59), and circulating FGF21 has been proposed as biomarker for primary muscle-manifest-

Fig. 8. Browning of WAT due to muscle secretion of FGF21. *A*: representative microscopy images (hematoxylin and eosin staining) of sWAT (*top*) and epididymal WAT (eWAT; *bottom*) from a WT and a UCP1-Tg mouse. Scale bars, 50 μm. *B*: qPCR analysis of brown fat marker genes in sWAT (*top*) and eWAT (*bottom*) of WT and UCP1-Tg mice. *C*: representative immunoblot image of respiratory chain complex proteins and UCP1 from sWAT of WT and UCP1-Tg mice (α-tubulin was used as a control). *D*: cytochrome *c* oxidase (COX) activity measured in sWAT of WT and UCP1-Tg mice. *E*: qPCR analysis of native UCP1 gene expression in muscle, BAT, and sWAT of WT and UCP1-Tg mice *F*: in vitro induction of UCP1 gene expression in primary white adipocytes incubated with 20% serum from WT or UCP1-Tg mice ± 2 μg of mouse FGF21 antibody (mFGF21-Ab). $*P < 0.05$, $**P < 0.01$, and $***P < 0.0001$, significant differences between the genotypes; $n = 6–8$/group, except for *F*, where $n = 3$. Data are means ± SE.

ing respiratory chain deficiencies in humans (56). We found a several-hundred-fold increase of FGF21 gene expression in SM of UCP1-Tg mice, resulting in five- to 10-fold elevated plasma levels compared with WT, which was considerably higher than levels detected in mice with a mitochondrial myopathy (59). In contrast to liver, there is no induction of FGF21 gene expression by 24-h fasting in SM (59), suggesting that the induction requires a more sustained stress insult than that provided by acute fasting and that different signaling pathways are involved in the secretion of FGF21 from liver and SM. Recently, we reported increased levels of lipid peroxidative damage and molecular stress markers (such as MAPK signaling and heat shock protein 25) linked to an upregulation of antioxidative defense (catalase and superoxide dismutase activity) in SM of UCP1-Tg mice (33). Here, we show additionally an activation of the p-eIF2α/ATF4 cascade that is part of the ISR, a gene-expression regulating program involved in substrate metabolism and cellular stress response (12). Recent studies in autophagy-deficient muscle have implicated this cascade in the induction of FGF21 gene expression due to mitochondrial dysfunction (37). Moreover, they showed that mitochondrial stressors also induce FGF21 through ATF4. Our results are supportive of this notion, and we propose the p-eIF2α/ATF4 cascade as a signaling pathway leading to the high FGF21 induction in SM of UCP1-Tg mice. Furthermore, increased mitochondrial ROS production does not seem to be necessary for FGF21 induction in SM, as evident from our in vitro treatment of C_2C_{12} cells with different inhibitors of the respiratory chain.

Remarkably, UCP1-Tg mice showed no evidence for a myopathy despite decreased muscle mass and rather an activated than inhibited autophagic machinery, but without increased basal autophagy flux. In any case, FGF21 expression in muscle is not purely a consequence of pathological impairment of autophagy processes or dystrophic morphology in muscle. Moreover, our data support the notion that increased FGF21 levels reflect a protective response. Altogether, our data show that FGF21 secretion from muscle is related to altered mitochondrial function and metabolic stress.

It has been suggested that FGF21 functions predominantly in a paracrine/autocrine manner because, so far, target tissues have also been the main tissues of FGF21 expression (35). Our data suggest that FGF21 secreted from muscle acts as a true endocrine hormone, targeting tissues other than the secreting tissue. There seems to be no autocrine/paracrine effect of FGF21 itself on muscle, as evident from the absent protein expression of KLB, the coreceptor required for FGF21 action. This fits with the report that overall muscle gene expression levels were affected very little by overexpression of FGF21 in transgenic mice (63). The main target organs of FGF21 are considered to be liver and adipose tissue (35), which is consistent with the expression pattern of KLB observed in our study. However, although we found little evidence for metabolic effects on liver, most pronounced metabolic changes were observed in WAT depots of UCP1-Tg mice.

Analysis of known downstream targets of FGF21 in WAT confirmed an activation of lipolysis, as reported previously (11). However, downstream signaling of FGF21 in WAT needs to be further investigated in view of discrepancies in the literature, especially with regard to ERK activation as well as the prevention of sumoylation and restoration of PPARγ activity by FGF21 (1, 11, 16, 23, 48).

Altogether, our data show that endocrine-acting FGF21 released by muscle leads to a browning of WAT. We further show that this effect is present not only in subcutaneous (inguinal) depots but also in gonadal (epididymal) WAT, where browning is rarely observed (54). Bearing in mind the concomitant age-dependent decrease of both browning and plasma FGF21 levels, it is interesting to speculate to what extent the browning effects and increased respiratory capacity in WAT are responsible for the positive metabolic actions of FGF21. It is very difficult to estimate the contribution of BAT-like cells within WAT to overall energy and substrate metabolism. It seems that browning of WAT represents a metabolic rather than a thermogenic adaptation, since the latter would be obtained much more efficiently by increasing BAT thermogenesis itself. We detected an increased futile cycle of lipogenesis and lipolysis in WAT of UCP1-Tg mice, which is also observed in WAT during cold exposure (4). Barneda et al. (4) speculated that this molecular mechanism is responsible for the transformation from unilocular to multilocular lipid droplets during the browning process. On the other hand, the induction of a futile cycle of lipogenesis and lipolysis could result in increased release of fatty acids, providing an additional fuel for SM, which shows not only an increased glucose uptake but also an increased fatty acid oxidation in UCP1-Tg mice (33, 50). Recently, it was speculated that FGF21 might enhance nutrient uptake in adipose tissue to channel substrates away from muscle to alleviate any extra metabolic stress caused by an overload of dietary nutrients (20). Here, we propose a quite opposite explanation. Our new data suggest that FGF21 is central to a metabolic rescue cycle aiming to channel substrates from peripheral tissues to SM rather than away from it. Very recent data suggest that FGF21's effects on liver and muscle are mediated by adiponectin released from WAT (40). However, UCP1-Tg mice do not show elevated adiponectin levels (50), which is consistent with the apparent absence of FGF21-induced effects on liver and muscle in UCP1-Tg mice.

Thus far, the positive health effects and increased longevity of UCP1-Tg mice had been attributed to an elevated metabolism of muscle itself (22, 34). This view is severely challenged by our new data showing that virtually all of the metabolic effects can be explained by the massive induction and secretion of FGF21 from SM, although we did not analyze UCP1-Tg/FGF21-knockout mice, which would be the ultimate proof for the causal role of FGF21 for the metabolic phenotype of UCP1-Tg mice. However, the phenotype of UCP1-Tg mice (i.e., reduced linear growth linked to reduced circulating IGF-I, reduced bone mass, increased energy expenditure and food intake, delayed development of obesity, reduced hepatic steatosis, improved glucose homeostasis, browning and activation of futile cycling in WAT, and even increased longevity) mirrors exactly the phenotype observed in FGF21-treated or FGF21-overexpressing mice (3, 19, 29, 63). Moreover, the in vitro experiments using primary WAT adipocytes clearly show the dependence of UCP1 induction in WAT on FGF21 action. Furthermore, fibronectin type III domain-containing 5/irisin, the only other myokine reported to induce WAT browning (6), is not upregulated in muscle of UCP1-Tg. Besides FGF21, IL-6 gene expression shows a much lower but significant upregula-

tion in SM of UCP1-Tg mice. This could be associated with increased muscle atrophy (24). Functional confirmation as well as elucidation of the molecular mechanism of IL-6 induction in muscle through mitochondrial uncoupling is a topic of future research.

In summary, our data suggest increased FGF21 secreted from muscle as a protective stress response and, furthermore, SM as an important endocrine regulator of whole body metabolism ultimately increasing longevity. These results open up new avenues of investigation that may help to resolve FGF21 function and regulation in humans, which is at present hardly understood.

ACKNOWLEDGMENTS

We thank Antje Sylvester, Carolin Borchert, Maria Kutschke, and Inge van der Stelt for technical assistance.

GRANTS

This research received funding from the European Union's Seventh Framework Program FP7 2007–2013 under grant agreement no. 244995 (BIOCLAIMS Project) and from the German Research Foundation (DFG: KL613/14-2).

DISCLOSURES

There are no conflicts of interest, financial or otherwise, for any of the authors.

AUTHOR CONTRIBUTIONS

S. Keipert, M.O., and S. Klaus contributed to the conception and design of the research; S. Keipert, M.O., K.J., and F.I. performed the experiments; S. Keipert, M.O., K.J., and F.I. analyzed the data; S. Keipert, M.O., M.J., E.M.V.S., J.K., and S. Klaus interpreted the results of the experiments; S. Keipert and M.O. prepared the figures; S. Keipert, M.O., M.J., E.M.V.S., J.K., and S. Klaus edited and revised the manuscript; S. Keipert, M.O., M.J., and S. Klaus approved the final version of the manuscript; S. Klaus drafted the manuscript.

REFERENCES

1. **Adams AC, Coskun T, Cheng CC, O Farrell LS, Dubois SL, Kharitonenkov A.** Fibroblast growth factor 21 is not required for the antidiabetic actions of the thiazoladinediones. *Mol Metab* 2: 205–214, 2013.
2. **Adams AC, Coskun T, Rovira AR, Schneider MA, Raches DW, Micanovic R, Bina HA, Dunbar JD, Kharitonenkov A.** Fundamentals of FGF19 & FGF21 action in vitro and in vivo. *PLoS One* 7: e38438, 2012.
3. **Badman MK, Pissios P, Kennedy AR, Koukos G, Flier JS, Maratos-Flier E.** Hepatic fibroblast growth factor 21 is regulated by PPARalpha and is a key mediator of hepatic lipid metabolism in ketotic states. *Cell Metab* 5: 426–437, 2007.
4. **Barneda D, Frontini A, Cinti S, Christian M.** Dynamic changes in lipid droplet-associated proteins in the "browning" of white adipose tissues. *Biochim Biophys Acta* 1831: 924–933, 2013.
5. **Boqué N, Campión J, Paternain L, García-Díaz DF, Galarraga M, Portillo MP, Milagro FI, Ortiz de Solórzano C, Martínez JA.** Influence of dietary macronutrient composition on adiposity and cellularity of different fat depots in Wistar rats. *J Physiol Biochem* 65: 387–395, 2009.
6. **Boström P, Wu J, Jedrychowski MP, Korde A, Ye L, Lo JC, Rasbach KA, Boström EA, Choi JH, Long JZ, Kajimura S, Zingaretti MC, Vind BF, Tu H, Cinti S, Højlund K, Gygi SP, Spiegelman BM.** A PGC1-α-dependent myokine that drives brown-fat-like development of white fat and thermogenesis. *Nature* 481: 463–468, 2012.
7. **Cantó C, Auwerx J.** Cell biology. FGF21 takes a fat bite. *Science* 336: 675–676, 2012.
8. **Coskun T, Bina HA, Schneider MA, Dunbar JD, Hu CC, Chen Y, Moller DE, Kharitonenkov A.** Fibroblast growth factor 21 corrects obesity in mice. *Endocrinology* 149: 6018–6027, 2008.
9. **Couplan E, Gelly C, Goubern M, Fleury C, Quesson B, Silberberg M, Thiaudiere E, Mateo P, Lonchampt M, Levens N, De Montrion C, Ortmann S, Klaus S, Gonzalez-Barroso MD, Cassard-Doulcier AM, Ricquier D, Bigard AX, Diolez P, Bouillaud F.** High level of uncoupling protein 1 expression in muscle of transgenic mice selectively affects muscles at rest and decreases their IIb fiber content. *J Biol Chem* 277: 43079–43088, 2002.
10. **Crofts AR, Barquera B, Gennis RB, Kuras R, Guergova-Kuras M, Berry EA.** Mechanism of ubiquinol oxidation by the bc(1) complex: different domains of the quinol binding pocket and their role in the mechanism and binding of inhibitors. *Biochemistry* 38: 15807–15826, 1999.
11. **De Sousa-Coelho AL, Relat J, Hondares E, Pérez-Martí A, Ribas F, Villarroya F, Marrero PF, Haro D.** FGF21 mediates the lipid metabolism response to amino acid starvation. *J Lipid Res* 54: 1786–1797, 2013.
12. **Dey S, Baird TD, Zhou D, Palam LR, Spandau DF, Wek RC.** Both transcriptional regulation and translational control of ATF4 are central to the integrated stress response. *J Biol Chem* 285: 33165–33174, 2010.
13. **Díaz-Delfín J, Hondares E, Iglesias R, Giralt M, Caelles C, Villarroya F.** TNF-α represses β-Klotho expression and impairs FGF21 action in adipose cells: involvement of JNK1 in the FGF21 pathway. *Endocrinology* 153: 4238–4245, 2012.
14. **Ding X, Boney-Montoya J, Owen BM, Bookout AL, Coate KC, Mangelsdorf DJ, Kliewer SA.** βKlotho is required for fibroblast growth factor 21 effects on growth and metabolism. *Cell Metab* 16: 387–393, 2012.
15. **Domouzoglou EM, Maratos-Flier E.** Fibroblast growth factor 21 is a metabolic regulator that plays a role in the adaptation to ketosis. *Am J Clin Nutr* 93: 901S–905S, 2011.
16. **Dutchak PA, Katafuchi T, Bookout AL, Choi JH, Yu RT, Mangelsdorf DJ, Kliewer SA.** Fibroblast growth factor-21 regulates PPARgamma activity and the antidiabetic actions of thiazolidinediones. *Cell* 148: 556–567, 2012.
17. **Fisher FM, Chui PC, Antonellis PJ, Bina HA, Kharitonenkov A, Flier JS, Maratos-Flier E.** Obesity is a fibroblast growth factor 21 (FGF21)-resistant state. *Diabetes* 59: 2781–2789, 2010.
18. **Fisher FM, Estall JL, Adams AC, Antonellis PJ, Bina HA, Flier JS, Kharitonenkov A, Spiegelman BM, Maratos-Flier E.** Integrated regulation of hepatic metabolism by fibroblast growth factor 21 (FGF21) in vivo. *Endocrinology* 152: 2996–3004, 2011.
19. **Fisher FM, Kleiner S, Douris N, Fox EC, Mepani RJ, Verdeguer F, Wu J, Kharitonenkov A, Flier JS, Maratos-Flier E, Spiegelman BM.** FGF21 regulates PGC-1alpha and browning of white adipose tissues in adaptive thermogenesis. *Genes Dev* 26: 271–281, 2012.
20. **Fisher FM, Maratos-Flier E.** Stress heats up the adipocyte. *Nat Med* 19: 17–18, 2013.
21. **Fon Tacer K, Bookout AL, Ding X, Kurosu H, John GB, Wang L, Goetz R, Mohammadi M, Kuro-o M, Mangelsdorf DJ, Kliewer SA.** Research resource: Comprehensive expression atlas of the fibroblast growth factor system in adult mouse. *Mol Endocrinol* 24: 2050–2064, 2010.
22. **Gates AC, Bernal-Mizrachi C, Chinault SL, Feng C, Schneider JG, Coleman T, Malone JP, Townsend RR, Chakravarthy MV, Semenkovich CF.** Respiratory uncoupling in skeletal muscle delays death and diminishes age-related disease. *Cell Metab* 6: 497–505, 2007.
23. **Ge X, Chen C, Hui X, Wang Y, Lam KS, Xu A.** Fibroblast growth factor 21 induces glucose transporter-1 expression through activation of the serum response factor/Ets-like protein-1 in adipocytes. *J Biol Chem* 286: 34533–34541, 2011.
24. **Haddad F, Zaldivar F, Cooper DM, Adams GR.** IL-6-induced skeletal muscle atrophy. *J Appl Physiol* 98: 911–917, 2005.
25. **He C, Bassik MC, Moresi V, Sun K, Wei Y, Zou Z, An Z, Loh J, Fisher J, Sun Q, Korsmeyer S, Packer M, May HI, Hill JA, Virgin HW, Gilpin C, Xiao G, Bassel-Duby R, Scherer PE, Levine B.** Exercise-induced BCL2-regulated autophagy is required for muscle glucose homeostasis. *Nature* 481: 511–515, 2012.
26. **Hojman P, Pedersen M, Nielsen AR, Krogh-Madsen R, Yfanti C, Akerstrom T, Nielsen S, Pedersen BK.** Fibroblast growth factor-21 is induced in human skeletal muscles by hyperinsulinemia. *Diabetes* 58: 2797–2801, 2009.
27. **Iglesias P, Selgas R, Romero S, Diez JJ.** Biological role, clinical significance, and therapeutic possibilities of the recently discovered metabolic hormone fibroblastic growth factor 21. *Eur J Endocrinol* 167: 301–309, 2012.
28. **Inagaki T, Dutchak P, Zhao G, Ding X, Gautron L, Parameswara V, Li Y, Goetz R, Mohammadi M, Esser V, Elmquist JK, Gerard RD, Burgess SC, Hammer RE, Mangelsdorf DJ, Kliewer SA.** Endocrine

regulation of the fasting response by PPARalpha-mediated induction of fibroblast growth factor 21. *Cell Metab* 5: 415–425, 2007.
29. **Inagaki T, Lin VY, Goetz R, Mohammadi M, Mangelsdorf DJ, Kliewer SA.** Inhibition of growth hormone signaling by the fasting-induced hormone FGF21. *Cell Metab* 8: 77–83, 2008.
30. **Johansen T, Lamark T.** Selective autophagy mediated by autophagic adapter proteins. *Autophagy* 7: 279–296, 2011.
31. **Kabeya Y, Mizushima N, Ueno T, Yamamoto A, Kirisako T, Noda T, Kominami E, Ohsumi Y, Yoshimori T.** LC3, a mammalian homologue of yeast Apg8p, is localized in autophagosome membranes after processing. *EMBO J* 19: 5720–5728, 2000.
32. **Katterle Y, Keipert S, Hof J, Klaus S.** Dissociation of obesity and insulin resistance in transgenic mice with skeletal muscle expression of uncoupling protein 1. *Physiol Genomics* 32: 352–359, 2008.
33. **Keipert S, Ost M, Chadt A, Voigt A, Ayala V, Portero-Otin M, Pamplona R, Al-Hasani H, Klaus S.** Skeletal muscle uncoupling-induced longevity in mice is linked to increased substrate metabolism and induction of the endogenous antioxidant defense system. *Am J Physiol Endocrinol Metab* 304: E495–E506, 2013.
34. **Keipert S, Voigt A, Klaus S.** Dietary effects on body composition, glucose metabolism, and longevity are modulated by skeletal muscle mitochondrial uncoupling in mice. *Aging Cell* 10: 122–136, 2011.
35. **Kharitonenkov A, Larsen P.** FGF21 reloaded: challenges of a rapidly growing field. *Trends Endocrinol Metab* 22: 81–86, 2011.
36. **Kharitonenkov A, Shiyanova TL, Koester A, Ford AM, Micanovic R, Galbreath EJ, Sandusky GE, Hammond LJ, Moyers JS, Owens RA, Gromada J, Brozinick JT, Hawkins ED, Wroblewski VJ, Li DS, Mehrbod F, Jaskunas SR, Shanafelt AB.** FGF-21 as a novel metabolic regulator. *J Clin Invest* 115: 1627–1635, 2005.
37. **Kim KH, Jeong YT, Oh H, Kim SH, Cho JM, Kim YN, Kim SS, Kim do H, Hur KY, Kim HK, Ko T, Han J, Kim HL, Kim J, Back SH, Komatsu M, Chen H, Chan DC, Konishi M, Itoh N, Choi CS, Lee MS.** Autophagy deficiency leads to protection from obesity and insulin resistance by inducing Fgf21 as a mitokine. *Nat Med* 19: 83–92, 2013.
38. **Klaus S, Rudolph B, Dohrmann C, Wehr R.** Expression of uncoupling protein 1 in skeletal muscle decreases muscle energy efficiency and affects thermoregulation and substrate oxidation. *Physiol Genomics* 21: 193–200, 2005.
39. **Komatsu M, Waguri S, Koike M, Sou YS, Ueno T, Hara T, Mizushima N, Iwata J, Ezaki J, Murata S, Hamazaki J, Nishito Y, Iemura S, Natsume T, Yanagawa T, Uwayama J, Warabi E, Yoshida H, Ishii T, Kobayashi A, Yamamoto M, Yue Z, Uchiyama Y, Kominami E, Tanaka K.** Homeostatic levels of p62 control cytoplasmic inclusion body formation in autophagy-deficient mice. *Cell* 131: 1149–1163, 2007.
40. **Lin Z, Tian H, Lam KS, Lin S, Hoo RC, Konishi M, Itoh N, Wang Y, Bornstein SR, Xu A, Li X.** Adiponectin mediates the metabolic effects of FGF21 on glucose homeostasis and insulin sensitivity in mice. *Cell Metab* 17: 779–789, 2013.
41. **Lundasen T, Hunt MC, Nilsson LM, Sanyal S, Angelin B, Alexson SE, Rudling M.** PPARalpha is a key regulator of hepatic FGF21. *Biochem Biophys Res Commun* 360: 437–440, 2007.
42. **Marciniak SJ, Ron D.** Endoplasmic reticulum stress signaling in disease. *Physiol Rev* 86: 1133–1149, 2006.
43. **Masiero E, Agatea L, Mammucari C, Blaauw B, Loro E, Komatsu M, Metzger D, Reggiani C, Schiaffino S, Sandri M.** Autophagy is required to maintain muscle mass. *Cell Metab* 10: 507–515, 2009.
44. **Meyer CW, Willershäuser M, Jastroch M, Rourke BC, Fromme T, Oelkrug R, Heldmaier G, Klingenspor M.** Adaptive thermogenesis and thermal conductance in wild-type and UCP1-KO mice. *Am J Physiol Regul Integr Comp Physiol* 299: R1396–R1406, 2010.
45. **Mizushima N, Komatsu M.** Autophagy: renovation of cells and tissues. *Cell* 147: 728–741, 2011.
46. **Mizushima N, Levine B, Cuervo AM, Klionsky DJ.** Autophagy fights disease through cellular self-digestion. *Nature* 451: 1069–1075, 2008.
47. **Muise ES, Azzolina B, Kuo DW, El-Sherbeini M, Tan Y, Yuan X, Mu J, Thompson JR, Berger JP, Wong KK.** Adipose fibroblast growth factor 21 is up-regulated by peroxisome proliferator-activated receptor gamma and altered metabolic states. *Mol Pharmacol* 74: 403–412, 2008.
48. **Muise ES, Souza S, Chi A, Tan Y, Zhao X, Liu F, Dallas-Yang Q, Wu M, Sarr T, Zhu L, Guo H, Li Z, Li W, Hu W, Jiang G, Paweletz CP, Hendrickson RC, Thompson JR, Mu J, Berger JP, Mehmet H.** Downstream signaling pathways in mouse adipose tissues following acute in vivo administration of fibroblast growth factor 21. *PLoS One* 8: e73011, 2013.
49. **Murata Y, Konishi M, Itoh N.** FGF21 as an Endocrine Regulator in Lipid Metabolism: From Molecular Evolution to Physiology and Pathophysiology. *J Nutr Metab* 2011: 981315, 2011.
50. **Neschen S, Katterle Y, Richter J, Augustin R, Scherneck S, Mirhashemi F, Schurmann A, Joost HG, Klaus S.** Uncoupling protein 1 expression in murine skeletal muscle increases AMPK activation, glucose turnover, and insulin sensitivity in vivo. *Physiol Genomics* 33: 333–340, 2008.
51. **Nishimura T, Nakatake Y, Konishi M, Itoh N.** Identification of a novel FGF, FGF-21, preferentially expressed in the liver. *Biochim Biophys Acta* 1492: 203–206, 2000.
52. **Pedersen BK, Febbraio MA.** Muscles, exercise and obesity: skeletal muscle as a secretory organ. *Nat Rev Endocrinol* 8: 457–465, 2012.
53. **Sandri M.** Autophagy in skeletal muscle. *FEBS Lett* 584: 1411–1416, 2010.
54. **Seale P, Conroe HM, Estall J, Kajimura S, Frontini A, Ishibashi J, Cohen P, Cinti S, Spiegelman BM.** Prdm16 determines the thermogenic program of subcutaneous white adipose tissue in mice. *J Clin Invest* 121: 96–105, 2011.
55. **Seebacher F, Guderley H, Elsey RM, Trosclair PL 3rd.** Seasonal acclimatisation of muscle metabolic enzymes in a reptile (Alligator mississippiensis). *J Exp Biol* 206: 1193–1200, 2003.
56. **Suomalainen A, Elo JM, Pietilainen KH, Hakonen AH, Sevastianova K, Korpela M, Isohanni P, Marjavaara SK, Tyni T, Kiuru-Enari S, Pihko H, Darin N, Ounap K, Kluijtmans LA, Paetau A, Buzkova J, Bindoff LA, Annunen-Rasila J, Uusimaa J, Rissanen A, Yki-Jarvinen H, Hirano M, Tulinius M, Smeitink J, Tyynismaa H.** FGF-21 as a biomarker for muscle-manifesting mitochondrial respiratory chain deficiencies: a diagnostic study. *Lancet Neurol* 10: 806–818, 2011.
57. **Svenning S, Lamark T, Krause K, Johansen T.** Plant NBR1 is a selective autophagy substrate and a functional hybrid of the mammalian autophagic adapters NBR1 and p62/SQSTM1. *Autophagy* 7: 993–1010, 2011.
58. **Turrens JF.** Superoxide production by the mitochondrial respiratory chain. *Biosci Rep* 17: 3–8, 1997.
59. **Tyynismaa H, Carroll CJ, Raimundo N, Ahola-Erkkila S, Wenz T, Ruhanen H, Guse K, Hemminki A, Peltola-Mjosund KE, Tulkki V, Oresic M, Moraes CT, Pietilainen K, Hovatta I, Suomalainen A.** Mitochondrial myopathy induces a starvation-like response. *Hum Mol Genet* 19: 3948–3958, 2010.
60. **Wei W, Dutchak PA, Wang X, Ding X, Bookout AL, Goetz R, Mohammadi M, Gerard RD, Dechow PC, Mangelsdorf DJ, Kliewer SA, Wan Y.** Fibroblast growth factor 21 promotes bone loss by potentiating the effects of peroxisome proliferator-activated receptor gamma. *Proc Natl Acad Sci USA* 109: 3143–3148, 2012.
61. **Weidberg H, Shvets E, Elazar Z.** Biogenesis and cargo selectivity of autophagosomes. *Annu Rev Biochem* 80: 125–156, 2011.
62. **Yakar S, Liu JL, Stannard B, Butler A, Accili D, Sauer B, LeRoith D.** Normal growth and development in the absence of hepatic insulin-like growth factor I. *Proc Natl Acad Sci USA* 96: 7324–7329, 1999.
63. **Zhang Y, Xie Y, Berglund ED, Coate KC, He TT, Katafuchi T, Xiao G, Potthoff MJ, Wei W, Wan Y, Yu RT, Evans RM, Kliewer SA, Mangelsdorf DJ.** The starvation hormone, fibroblast growth factor-21, extends lifespan in mice. *Elife* 1: e00065, 2012.
64. **Zhou D, Palam LR, Jiang L, Narasimhan J, Staschke KA, Wek RC.** Phosphorylation of eIF2 directs ATF5 translational control in response to diverse stress conditions. *J Biol Chem* 283: 7064–7073, 2008.